Supporting Online Material for

Counting Cytokinesis Proteins Globally and Locally in Fission Yeast

Jian-Qiu Wu and Thomas D. Pollard*

*To whom correspondence should be addressed. E-mail: thomas.pollard@yale.edu

Published 14 October 2005, *Science* **310**, 310 (2005)
DOI: 10.1126/science.1113230

This PDF file includes:

Counting Cytokinesis Proteins Globally and Locally in Fission Yeast

Jian-Qiu Wu and Thomas D. Pollard

Supporting Online Material

Contents

Materials and Methods

Strain construction and growth conditions

Supplemental Table S1 lists the *S. pombe* strains used in this study. Strains were constructed by PCR-based gene targeting (*S1, S2*) and confirmed by PCR over both junctions and in some cases across the whole integration fragment. All strains except that with YFP-actin plasmid (JW1206) expressed the fusion protein from its chromosomal locus under the control of its native promoter. Conventional myosin-II *myo2* and PCH protein *cdc15* were tagged at their N-termini leaving their native promoters in place (*S2*). The 5' UTR plus start codon ATG of *myo2* (-1,184 to +3) and *cdc15* (-433 to +3) were amplified and cloned into pFA6a vector digested with *Bgl* II and *Pac* I. The fidelity of the PCR inserts was confirmed by sequencing both strands. The resulting plasmids were pFA6a-kanMX6-Pmyo2-mYFP (JQW105) and pFA6a-kanMX6-Pcdc15-mYFP (JQW90). The gene-specific sequences of forward primers were from -95 to -15 upstream of ATG for *myo2*, and -85 to -5 for *cdc15*. Four repeats of TCC were added in the reverse primer for *cdc15* creating a linker of four-glycines between mYFP and the protein. To examine the effects of the *kanMX6* selectable marker on the protein levels of N-terminal-tagged proteins, we looped out the marker flanking with repeats of 5' UTR by backcrossing the geneticin-resistant (kan^r) strains to wt and selected geneticin-sensitive (kan^s) strains.

For genes tagged at their COOH termini, the gene-specific sequences of reverse primers ended downstream of the stop codon 83 bp for *ain1*, 7 bp for *cdc7*, 1 bp for *cdc12*, 4 bp for *chs2*, 68 bp for *fim1*, 7 bp for *mid1*, 5 bp for *mid2*, 3 bp for *pck2*, 12 bp for *plo1*, 1 bp for *rgf1*, 8 bp for *rgf3*, 1 bp for *sad1*, 28 bp for *spn1*, 44 bp for *spn4*. Plasmids pFA6a-mYFP-kanMX6 (JQW86), pFA6a-YFP-kanMX6 (JQW37; for genes *cdc7, acp2,* and *myp2*), and pFA6a-3YFP-kanMX6 (for *cdc12* and *rng3*) were used as templates in PCR to amplify DNAs for the gene targeting.

We chose YFP over GFP (except Mid2p-mEGFP) since the autofluorescence of wild type (wt) *S. pombe* cells is lower with excitation at 514 nm than at 488 nm, a critical

difference for measuring weak signals. We tested the functionalities of the tagged strains as described (*S2*). All tagged strains except *mYFP-cdc4* formed normal colonies and resembled wt cells in morphology from 18 to 36°C. Although the cell morphology of strain *mYFP-cdc4* was normal at 25°C, cells had cytokinesis defects at 36°C (*S2*). Because some dividing cells expressing Mid2p-mYFP (JW1169) or Mid2p-YFP formed a fluorescent aggregate, we used Mid2p-mEGFP (strain JW1213) to study the fluctuation of Mid2p across the cell cycle.

Cells were grown in exponential phase at 25°C in YE5S rich liquid medium in 50 ml flasks in the dark to a density of 2 to 10 x 10^6 for microscopy and 6.3 to 9.2 x 10^6 cells/ml for immunoblotting (measured by OD_{595}). To measure the YFP-actin concentration (Fig. 1E), we grew cells of strains JW1206 and wt JW729 in EMM minimal liquid medium for 36 h. After washing once with YE5S, the cells were grown in YE5S for another 4 h and then processed for microscopy and gel electrophoresis. Cells expressing Fim1p-mYFP were treated with Latrunculin A as described (*S2*).

Microscopy

Live cells in growth chambers (*S2*) were observed with a Plan-Apo 100X/1.4 NA objective on an UltraView RS spinning-disk confocal microscope (PerkinElmer Life and Analytical Sciences, Boston, MA) using a 514-nm argon ion laser (488 nm for strain JW1213 *mid2-mEGFP*) and emission filter 525 to 625 nm (peak at 575 nm). The refractive index of the immersion oil is 1.52. Fluorescence and differential-interference-contrast (DIC) images were collected with an ORCA-ER cooled CCD camera. The DIC images are compromised by the Piezo Z objective collar that increases the distance between the objective and the Wollaston prism and by their passing through the spinning pinhole disc. However, this does not affect the fluorescence measurements. To reduce photo-toxicity 0.1 ml 1.0 mM n-propyl-gallate (Sigma P-3130) made in YE5S was added to 0.9 ml cells. Cells were concentrated 10 to 20 fold by centrifugation at 4500 rpm for 5 to 10 sec and resuspended. Ten μl of cells were mounted on a thin layer of 100 μl 25% gelatin (Sigma; G-2500) in YE5S and 0.1 mM n-propyl-gallate, sealed under a coverslip with Valap, and observed at 23°C. Stacks of fluorescent images were collected with the same laser power and imaging settings (Fig. S2). The stability of the optical systems was confirmed by imaging several strains at both the beginning and the end of both experiments reported in Table 1. We varied the exposure time (Table 1) to optimize signal to noise and use the linear range of camera, minimize movements of spindle pole bodies and actin patches, avoid saturating camera, and minimize photo bleaching. Pixels were binned 2 x 2, and the gain was set at 15.7 dB (Decibel). The field size was 672 x 512 binned pixels (61.1 x 46.6 μm).

To determine the sampling interval along the Z-axis, we measured the spread of the image of a point source. We used the spinning disk confocal microscope to image quantum dots (Qdot 585 Streptavidin Conjugate; Quantum Dot Corporation, Hayward, CA) in all three directions. The intensity of a sample of these dots was spread out in approximately Gaussian distributions in both the X-Y plane and along the Z-axis. The Full Width Half Maximum (FWHM) of these distributions was 0.58 ± 0.08 μm in Z direction and 0.19 ± 0.03 μm in the X-Y plane. We used the assumption " the FWHM

approximates the z-dimensional thickness of the sample which contributes to fluorescence signal, and that the efficiency of detection of fluorescence within the volume is constant" (*S3*) to determine the intervals for the z-sections. Thus, we collected a stack of 12 confocal z-sections at intervals of 0.60 μm from 3 to 10 fields, which extended beyond the upper and lower edges of the cells, as required to collect all of the fluorescent signal. The contribution of out of focus fluorescence was included in both the calibration of the standard curve as well as the measurements of the global and local concentrations. Wt JW729 was imaged under the same conditions with exposure times spanning those used for the experimental strains.

To correct for uneven illumination, we mounted 20 μl purified 6His-mYFP at a range of concentrations on the gelatin pad and collected images from the middle portion of the solution. The offset pixel intensity at different exposures was obtained using the same setting as for cells but without the laser beam. To assess the effects of photobleaching, we measured the loss of fluorescence signal by collecting a series of Z-sections over the range of exposures that we used. Using a short exposure (69 msec per slice) the summed fluorescence declined exponentially about 8% per Z-stack. At 300 msec per slice, the intensity declined about 25% per Z-stack. Thus, we focused by DIC to avoid bleaching and limited our data collection to one Z-stack per field and no more than five stacks per slide.

Data analysis

We used Image J software (http://rsb.info.nih.gov/ij/) to sum the fluorescence intensity and correct for background and uneven illumination of each stack of images. Stacks of fluorescence images were projected into 2D images using a sum intensity projection. The offset pixel intensity of the same exposure time was subtracted from the sum images. To correct for uneven illumination, the offset subtracted sum images were divided by the correction image, the sum images of the 6His-mYFP solution divided by its maximal pixel intensity.

The inner boundaries of 42 to 302 cells (all cells in 3 to 10 fields) of each strain were marked on DIC images with the polygon selections tool in Image J. We found that area measured by marking the inner boundary of DIC images was the same as the real size by measuring 6-μm beads. The marked area and its mean pixel intensity were recorded and transferred to Microsoft Excel for analysis. The background fluorescence intensity of wt cells was a linear function of exposure time from 69 to 798 ms ($y = 0.9418x$, $R = 0.9995$; where y is mean pixel intensity per cell, and x is exposure time in msec; the standard deviation is less than 5% of the mean intensity at any exposure). This cellular background was subtracted from the intensity of cells with a fusion protein. We confirmed that mYFP is 1.1x brighter than YFP (*S4*) by measuring cells expressing mYFP-Myo2p (JW1110; $N = 59$ cells) and YFP-Myo2p (JW827; $N = 52$ cells). Thus, all background corrected mean intensities were normalized to that of 1 sec exposure for mYFP for comparison.

To measure local protein concentrations in contractile rings, septin rings, and SPBs, we used sum images and drew a rectangular or circular measuring area large enough to contain >95% fluorescence from the target. . At the division site the rectangle

width was typically 32 pixels (2.91 μm) for the broad band and 5-10 pixels for contractile rings or septin rings. The measuring circle was 8-pixels (0.73 μm) in diameter for SPBs. Around each measuring area a concentric box or circle with 2.1 times the area was drawn inside the cellular boundary to correct for background. For proteins (Cdc15p and Pck2p) that spread over the whole septum region during contraction, the length of small box was 2 pixels wider than the diameter of the contractile ring. For proteins in patches, the circles were 5 (inner) and 7 (outer) pixels in diameter, and intensity in three slices (not 2-D sum projection) were measured and summed. The total pixel intensity within these areas was measured. The fluorescence intensity within the measuring area was corrected for background by subtracting the intensity of the surrounding area (*S5*). The normalized 1 sec mYFP local intensity was converted to molecules according to the standard curve (Fig. 1C). Cell cycle phases were calculated or estimated by morphology of the contractile ring, contractile-ring diameter, septum diameter, and/or separation of SPBs, and assigned a cytokinesis time from our standard temporal pathway at 25°C (*S2*).

Cloning and purification of 6His-mYFP and immunoblotting

mYFP in pFA6a- mYFP-kanMX6 (JQW86) was amplified by PCR using primers 5'-ACG GAT CCC CCG GGT TAA TTA ACA GTA AAG G-3' (forward) and 5'-GTG GTC GAC CTA TTT GTA TAG TTC ATC CAT GC-3' (reverse) and cloned into pQE80 vector digested with *Bam*H I and *Sal* I to obtain the expression construct pQE80-6His-mYFP (JQW111). 6His-mYFP was purified from *E. coli* strain BL21 (DE3) pLysS (Novagen) grown in the dark at 25°C (*S6*). The eluate from Talon Metal Affinity Resin (BD Biosciences, Palo Alto, CA) was dialyzed (20 mM Tris, 25 mM NaCl, 1 mM DTT, and 0.01% NaN_3, pH 8.1) and applied to a 1-ml Mono-Q column (Amersham Biosciences, Piscataway, NJ) and eluted with a 75-ml linear gradient of 0.025-1 M NaCl in the above dialyzing buffer by FPLC. Pure 6His-mYFP was dialyzed into HEPES buffer at 4°C (20 mM HEPES, 50 mM KCl, 1 mM EDTA, 1 mM DTT, and 0.01% NaN_3, pH 7.5) and stored in a dialysis bag at 4°C with the buffer changed every 4 days. The mYFP concentration was determined by absorbance at 514 nm using an extinction coefficient of 79,000 M^{-1} cm^{-1} (*S4*).

For immunoblotting, cells in 13.5 ml YE5S were pelleted and the supernatant removed. The pellets (30 to 50 mg of wet cells) were suspended in ice-cold lysis buffer (50 mM HEPES, 100 mM KCl, 3 mM $MgCl_2$, 1 mM EGTA, 0.1% Triton X-100, 1 mM DTT, 1 mM PMSF, with one complete protease inhibitor tablet (Roche Diagnostics, Indianapolis, IN)/25 ml, pH 7.5) to a final volume of 300 μl, and then we added 0.3 g acid-washed glass beads (425-600 μm; Sigma). About 90% of cells were lysed (judging from DIC microscopy) by treatment in a Fastprep bead beater for 6 x 30 sec (5 min on ice between each run) at 4°C. After adding 150 μl boiling sample buffer (250 mM Tris-HCl, pH 6.8, 50% glycerol, 3.58 M β-mercaptoethanol, 15% SDS, and 0.025% Bromophenol Blue), samples were incubated at 100°C for 5 min. Samples were centrifuged at 14,000 rpm in a desktop centrifuge at room temperature for 10 min and 300 μl of supernatant were divided into 4 samples and stored at -80°C.

We measured the average number of molecules per cell by electrophoresis in 10 to 20% gradients of polyacrylamide in SDS and immunoblotting. Standard samples

consisted of 0.1 to 1.5 ng 6His-mYFP in either 5.0 (for Ain1p, Spn1p, Spn4p, and YFP-actin) or 1.0 µl (for Arc1p, Arp2p, Arp3p, and Fim1p) of cell extract from wt cells (JW729). Unknown samples on the same gels were of 5.0 and 2.5 µl of cell extract from strains expressing Ain1p-mYFP (JW1145), Spn1p-mYFP (JW1092) or Spn4p-mYFP (JW1171), or 1.0 and 0.5 µl of extract from strains expressing Arc1p-mYFP (CB108), Arp2p-mYFP (CB106), Arp3p-mYFP (CB107) or Fim1p-mYFP (JW1041), or 3 to 9 µl of cell extract from wt strain with YFP-actin plasmid (JW1206). The gels were run at 170 volts for 90 min, and proteins were transferred to PVDF membranes in transfer buffer (25 mM Tris-Base, 192 mM glycine, 0.04% SDS, 10% methanol) at a constant voltage of 23 volts overnight at 4°C. We monitored the transfer efficiency by staining all the gels after transfer and the membranes after ECL detection using GelCode Blue (# 24590, Pierce, Rockford, IL). Under these conditions, the vast majority of the proteins were transferred to the PVDF membranes. The blots were probed with BD Living Colors A.v. Monoclonal Antibody (JL-8) (BD Biosciences, 632380) against YFP (1:1,000) and then peroxidase-conjugated anti-mouse IgG (1:5,000; Sigma, A-4416). Blots were reacted with homemade ECL reagent and exposed to KODAK BioMax MR film, which were developed, scanned, and quantified using Image J. The YFP antibody detected a single or major band of the size expected for the fusion protein on immunoblots of strains expressing Acp2p-YFP (KV60), Arc5p-mYFP (CB71), mYFP-Cdc4p (JW910), mYFP-Cdc15p (JW1039), and mYFP-Myo2p (JW1110). No band corresponding to free YFP was detected even with very long exposures.

To measure the endogenous actin concentration, 0.25 to 1.0 µl of cell extract from wt strain with (JW1206) or without (JW729) the YFP-actin plasmid was loaded along with 0 to 42 ng purified *S. pombe* actin (*S7*) or rabbit skeletal muscle actin, alone or in 0.5 µl wt cell extract (JW729). Gels were run and transferred as described above. Blots were probed with monoclonal antibody C4 against chicken gizzard actin (1:2,000; a kind gift of James Lessard, University of Cincinnati Children's Hospital), processed and quantified as above.

To compare the expression Arp3p with and without the mYFP tag, 0.5 to 5.0 µl cell extracts from equal numbers of wt (JW729) and *arp3-mYFP* (CB107) cells were separated and transferred as above. The blot was probed with polyclonal antibodies against *S. pombe* Arp3p (1:10,000; a kind gift of Kathy Gould, Vanderbilt University) and then peroxidase-conjugated anti-rabbit IgG (1:10,000).

Flow cytometry

Cells expressing each YFP fusion protein were grown as described above to ~4 x 10^6 per ml. The fluorescence of ~10,000 cells was measured at a flow rate of ~1,000 cells per second with a FACSCalibur flow cytometer (BD Biosciences, Palo Alto, CA) using a 488 nm excitation and 530/30 bandpass filter. Data were analyzed using FlowJo software (Treestar, Inc, Ashland, OR).

Calculation volumes of whole cell, contractile ring, SPB, and actin patches

S. pombe cells have a regular rod shape with a constant diameter of D = 3.74 ± 0.15 µm (N = 2600 cells). We used the cell area (A) measured from DIC images to calculate cell

volumes. We divided a cell into a cylinder with a diameter (D) of 3.74 μm and a height H and two hemispheres with a diameter (D) of 3.74 μm. Thus, the average volume of asynchronous cells is 92 μm^3 (N = 658 cells). We used electron micrographs (*S8, S9*) of thin sections of quick-frozen, freeze-substituted cells to determine the volume of contractile ring. We measured the region of the contractile ring excluding ribosomes using Image J. The cross sectional area of actin filament bundle in the contractile ring was 0.027 ± 0.019 μm^2 (N = 10). We assumed the area did not change during constriction of the ring. Thus the volume (V) of contractile ring is $V = 0.027 \pi d$, where d is the diameter of contractile ring. To calculate the volume of the broad band (V), we assumed that proteins accumulated in a cortex layer with a thickness similar to the actin ring (0.19 μm). The cell diameter excluding cell wall is 3.46 μm from EM images. Thus, $V = \pi h [(3.46/2)^2 - [(3.46-0.19)/2]^2]$, where h is the width of the box when measuring broad band. SPBs are an oblate ellipsoids ~0.18 μm in diameter and 0.09 μm thick during most of the cell cycle and 0.05 μm thick in early mitosis (*S10, S11*). Thus the SPB volume is 1.53 or 0.85 x 10^{-3} μm^3. Actin patches are spherical with a diameter of 0.1 to 0.3 μm (*S12*). We assumed the diameter is 0.25 μm. Thus, the average volume of actin patches is 8.2 x 10^{-3} μm^3.

Estimation of cytoplasmic volume fraction by point counting stereology and actin filament in contractile ring

We used the point counting method to estimate the volume fraction of the various compartments in *S. pombe* cells from electron micrographs (*S8*) of thin sections of quick-frozen, freeze-substituted cells. A square grid of test points was positioned over each EM image and scored as being over one of four compartments: cytoplasm, ribosomes, membrane-bounded organelles, and cell wall. The technique is based on the principle that the ratio of the area of a compartment to that of the whole cell is proportional to the ratio of volume in random thin sections. We found that cytoplasm occupies 29% and the nucleus 12% of cell volume.

We estimated the actin filaments in the contractile ring using the published electron micrographs (Fig. 5, B and C in *S8*). The paper shows five clear filaments in one tangential section and one micrograph showing that the bundle of filaments is circular in cross section. Given a circular bundle with a maximum of 5 filaments in any plane, the entire ring has about 20 filaments.

Effects of the YFP tag and the *kanMX6* selectable marker on the protein levels

We found that the YFP tag and the *kanMX6* selectable marker had little effects on protein concentrations except for Cdc15p (Fig. S1). Immunoblotting using anti-Arp3p antibodies showed that cells expressed Arp3p-mYFP and wt Arp3p with no more than 10% difference (Fig. S1, A and B). The *kanMX6* selectable marker had no major effects on the mYFP-Myo2p and mYFP-Rng2p levels as measured by microscopy (Fig. S1, C and D). However, mYFP-Cdc15p concentration was ~65 or 95% higher in a strain with the *kanMX6* marker upstream of mYFP (strain JW1039) than in *mYFP-cdc15* strain without the marker (JW1063) or in *cdc15-mYFP* strain (JW977) with the *kanMX6* marker

downstream of mYFP (Fig. S1E). It was possible that the P_{TEF} promoter for the *kanMX6* marker (although in reverse direction) enhanced the transcription of *cdc15* mRNA.

Error assessment of our quantification

Independent measurements of the concentrations of subunits in two different complexes suggest that our measurements differ by less than a factor of two from the actual values for abundant proteins. The measured global concentrations of five of Arp2/3 complex subunits differ by a maximum 1.5 fold from the mean of the five measurements (Table 1). The local concentrations of these five subunits differ by less than 10% from the mean in actin patches (Fig. 2B). The subunits are present in equal molar amounts in the complex (*S13*) with little or no free subunits in *Acanthamoeba* (*S14*). The concentration of the myosin regulatory light chain Rlc1p was 72% of the total of Myo2p and Myp2p myosin-II heavy chains, its partners in the cell (*S15, S16*). However, for low abundance proteins, the accuracy is lower due to photobleaching from the longer exposures and to lower signal to noise ratios.

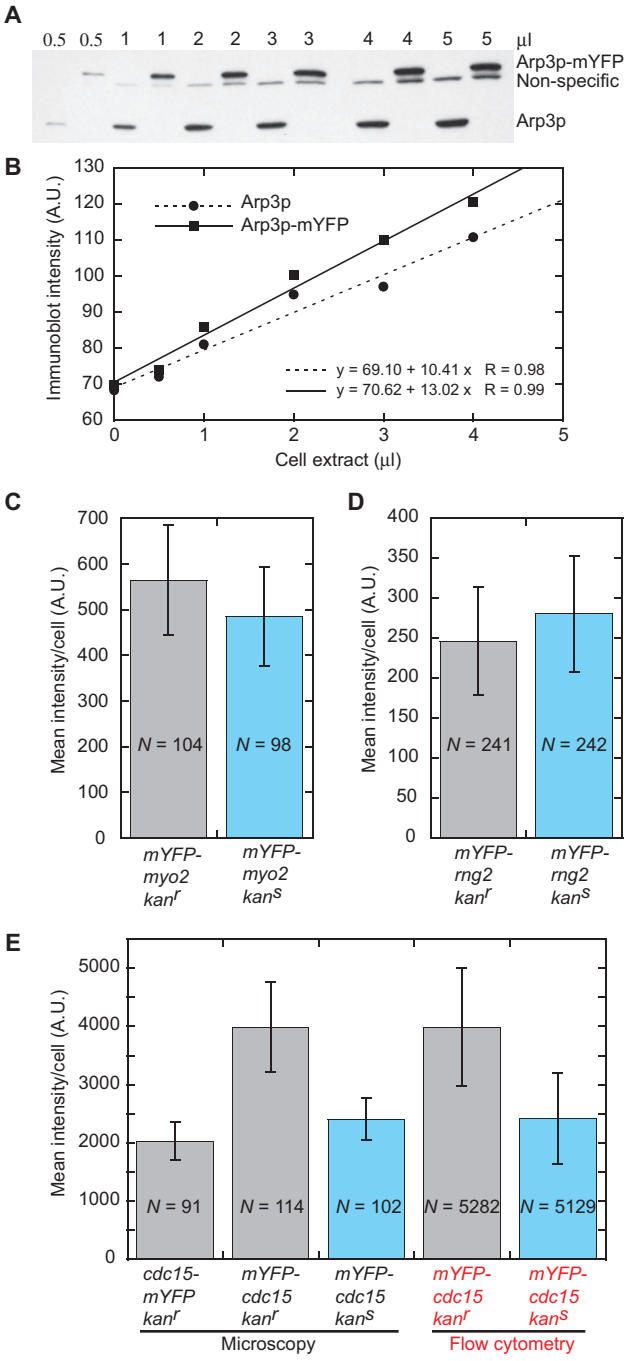

Fig. S1. Effects of YFP tag and the selectable marker *kanMX6* on protein expression. (**A** and **B**) Measurement of Arp3p concentration by quantitative immunoblotting. (**A**) Range of volumes of extracts from equal numbers of wt JW729 and *arp3-mYFP* (CB107) cells were separated by SDS-PAGE and probed using anti-Arp3p antibodies. (**B**) Dependence of the immunoblot intensity on sample size of blot in (A) measured by Image J and densitometry. (**C-E**) Effects of the selectable marker *kanMX6* in endogenous genes on the expressions of (C) mYFP-Myo2p, (D) mYFP-Rng2p, and (E) Cdc15p-mYFP and mYFP-Cdc15p measured by fluorescence microscopy or flow cytometry. Cell-size corrected integrated mYFP fluorescence intensities per cell (mean ± 1 standard deviation) from indicated number of cells are shown.

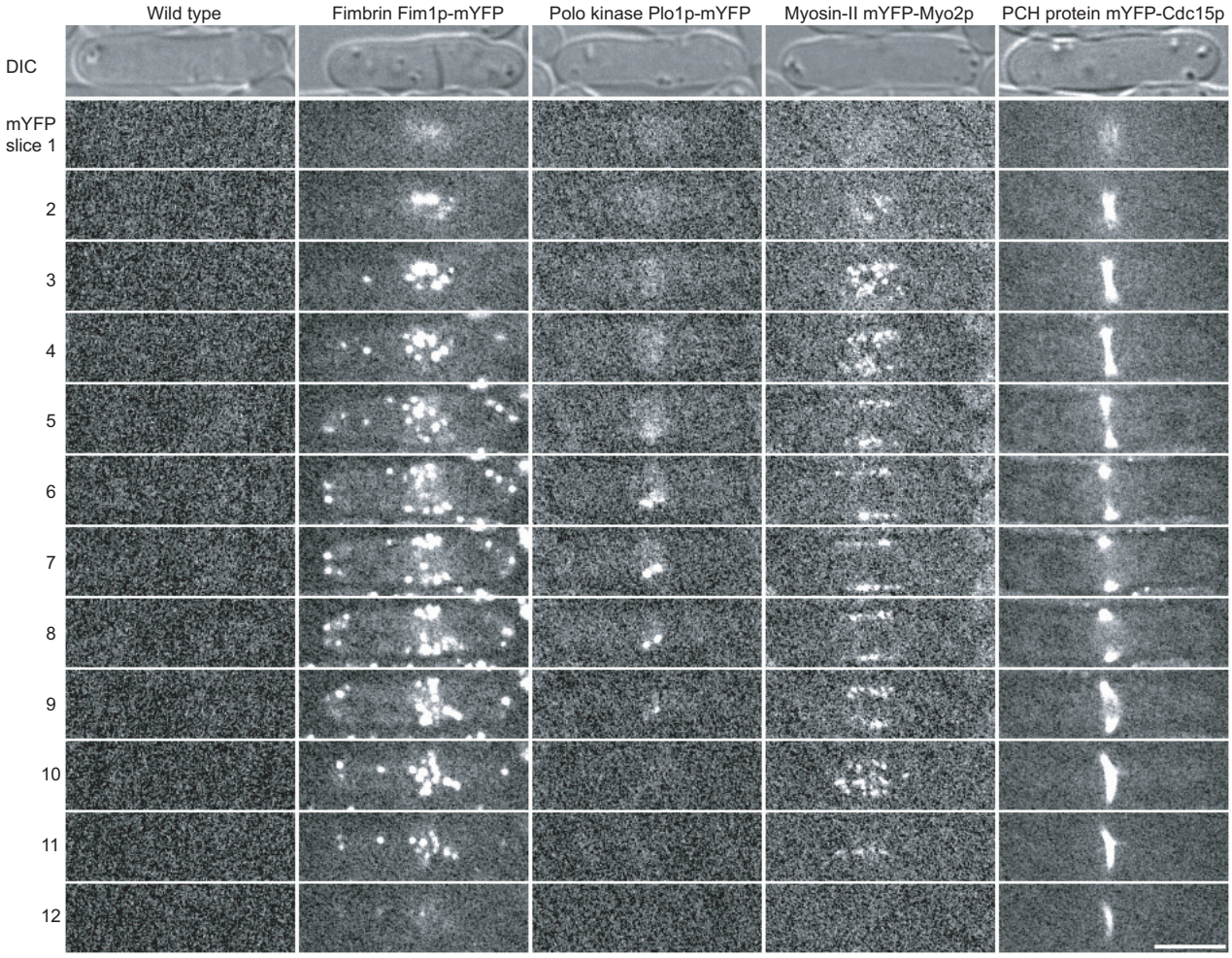

Fig. S2. Raw DIC and fluorescence images of living wt cells (strain JW729) and cells expressing integrated fimbrin Fim1p-mYFP (JW1041), polo kinase Plo1p-mYFP (JW1107), myosin-II mYFP-Myo2p (JW1110), PCH protein mYFP-Cdc15p (JW1063) at their endogenous levels. The fluorescence micrographs of 12 Z-sections spaced at 0.6 μm intervals were taken using the exposure times listed in Table 1 (399 msec for wt). Scale bar, 5 μm.

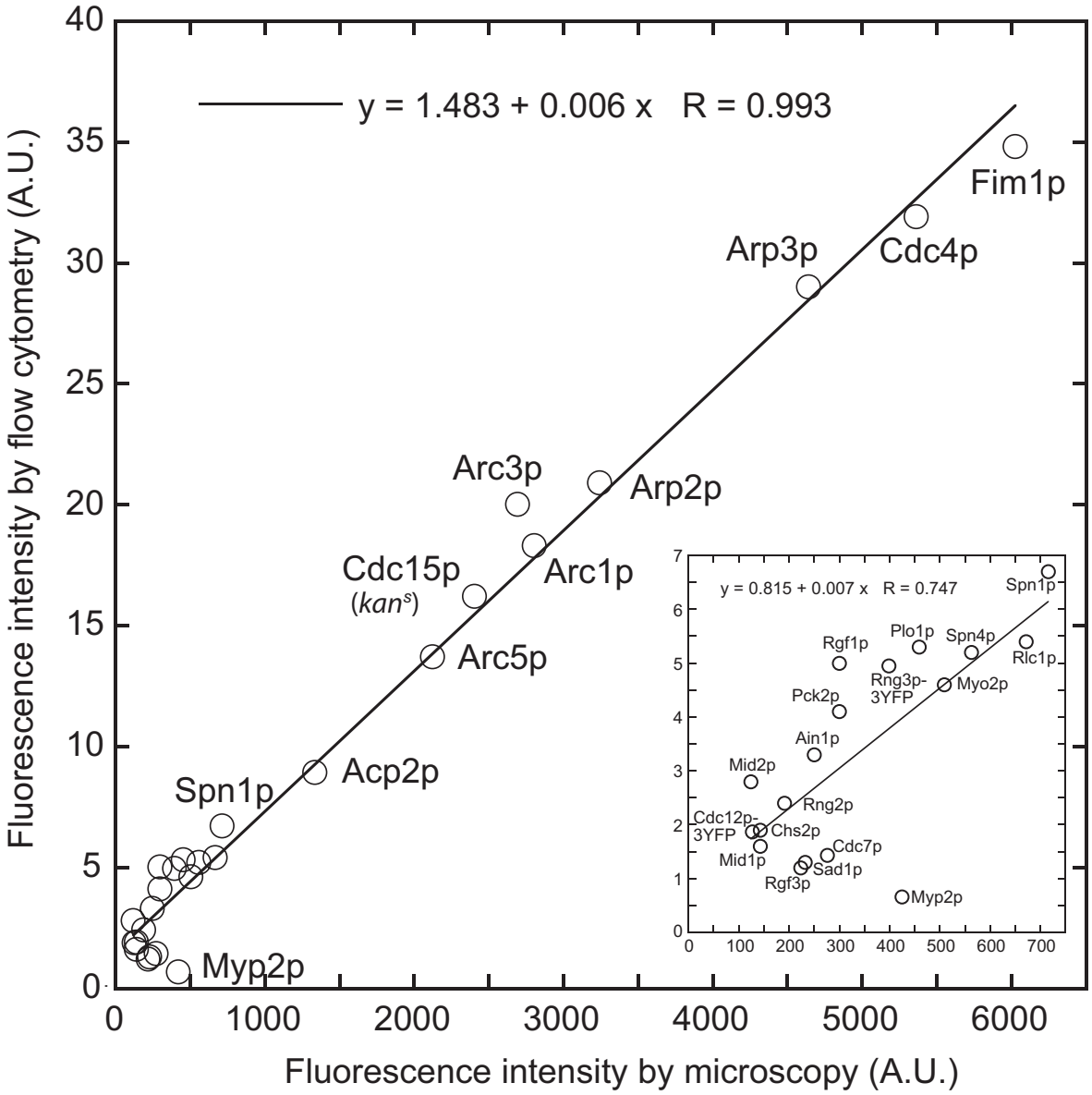

Fig. S3. The linear relationship between the fluorescence intensity measured by microscopy and flow cytometry. The correlation of mean integrated fluorescence intensity per cell from microscopy and flow cytometry for strains expressing integrated YFP or mYFP fusion proteins. Each symbol represents a fusion protein. The inset shows the correlation of the low abundance proteins.

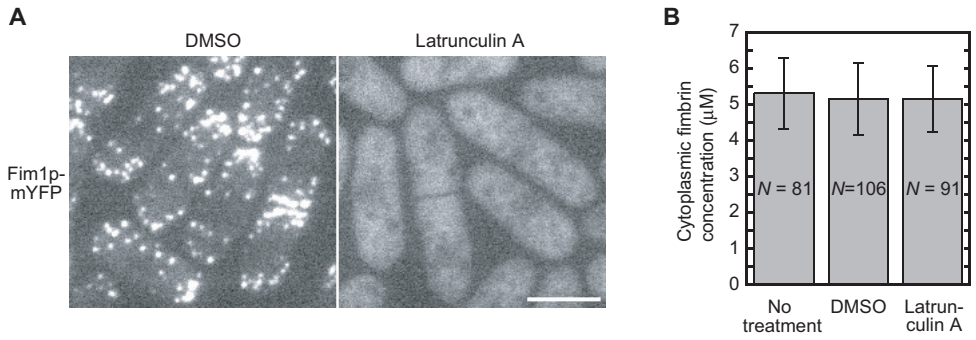

Fig. S4. Lack of effect of Latrunculin A on the total fluorescence of cells expressing Fim1p-mYFP. Cells were treated with DMSO or 100 μM Latrunculin A. (A) Stacks of fluorescence micrographs from 12 z-sections spaced at 0.6 μm intervals taken using same exposure time were projected into a 2D image using a sum intensity projection. Scale bar, 5 μm. (B) Mean global cytoplasmic concentration ± 1 standard deviation of number of cells indicated for each condition.

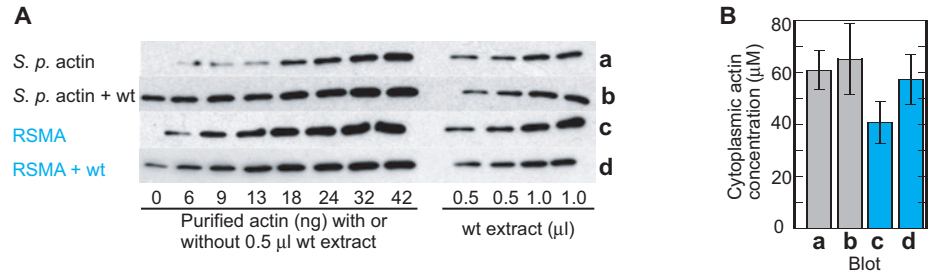

Fig. S5. Measurements of actin concentration by quantitative immunoblotting with internal standards and anti-actin antibody. (**A**) Immunoblots of samples probed with anti-actin antibody. All four experiments have duplicate samples of wt cells JW729 grown in YE5S. (**a**) Range of purified *S. pombe* actin. (**b**) Range of purified *S. pombe* actin in 0.5 μl of extract of wt cells. (**c**) Range of purified rabbit skeletal muscle actin (**d**) Range of purified rabbit skeletal muscle actin in 0.5 μl of extract of wt cells. (**B**) Quantitation of cytoplasmic actin concentration (mean ± 1 standard deviation) of blots in (A) by Image J and densitometry.

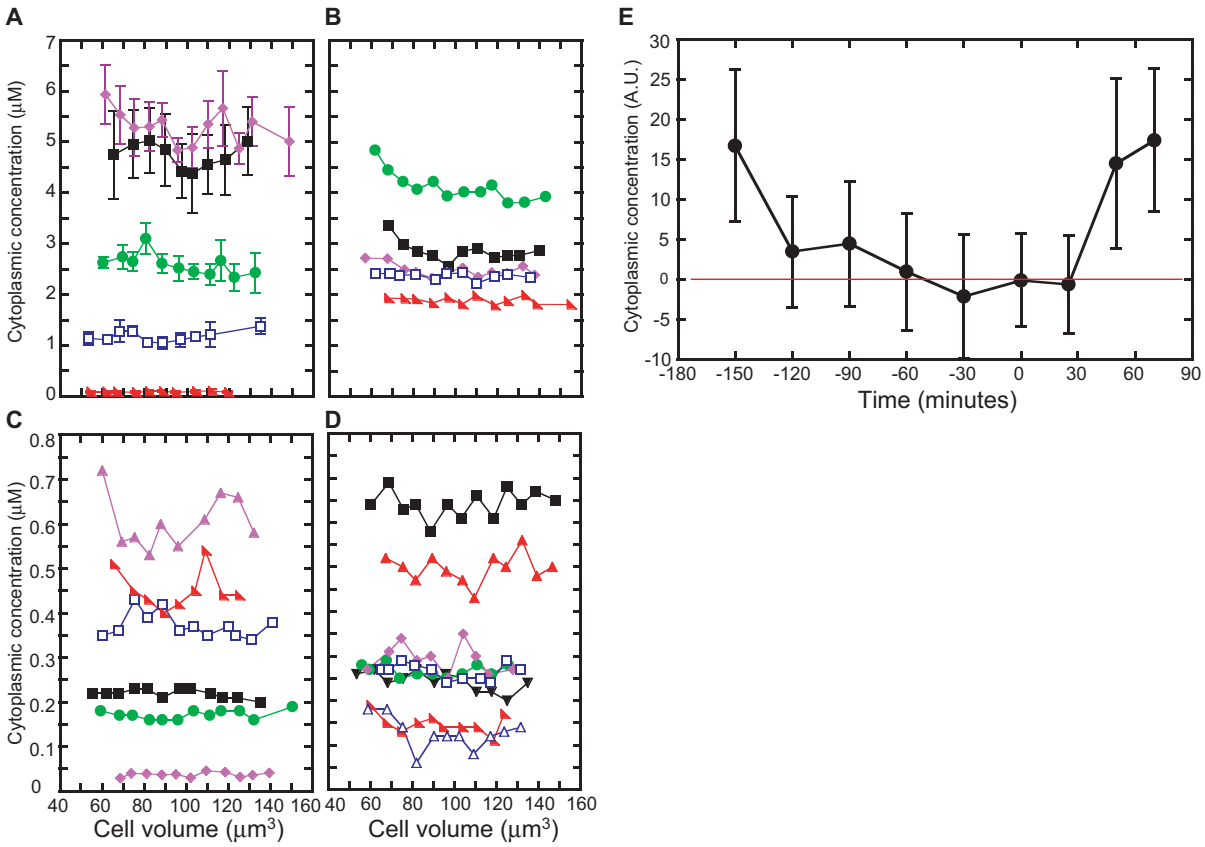

Fig. S6. Cytoplasmic protein concentrations across the cell cycle measured by fluorescence microscopy. (A-D) Measurements of cytoplasmic protein concentrations of 42 to 159 cells (Table 1) were binned at increments of cell volume of ~7.0 μm^3. The means for these smaller samples are graphed versus cell volume, a scale for cell-cycle stage. Standard deviations are included in (A and E) and omitted from (B, C, and D) for clarity.
(**A**) (♦) Fim1p, (■) Cdc4p, (●) Cdc15p, (□) Acp2p, and (◣) Mid1p.
(**B**) (●) Arp3p, (■) Arp2p, (♦) Arc1p, (□) Arc3p, and (◣) Arc5p.
(**C**) (▲) Rlc1p, (◣) Myo2p, (□) Myp2p, (■) Ain1p, (●) Rng2p, and (♦) Cdc12p.
(**D**) (■) Spn1p, (▲) Spn4p, (♦) Plo1p, (□) Rgf1p, (●) Pck2p, (▼) Cdc7p, (◣) Sad1p, and (Δ) Chs2p.
(**E**) Fluctuation of the mean fluorescence (± 1 standard deviation) of the anillin-like protein Mid2p-mEGFP (strain JW1213) across the cell cycle. The scale is arbitrary since GFP fluorescence is not calibrated. The red line is zero. Onset of mitosis is defined as time zero and -150 min as the birth of daughter cells. The cell-cycle times of cells (*N* = 124 cells) were estimated from cell volumes and the morphology and diameter of septum.

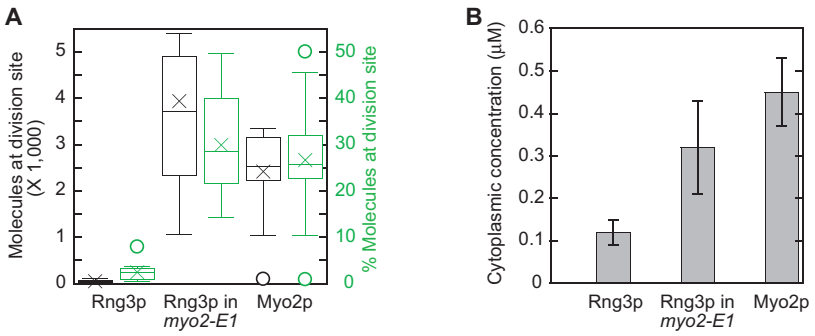

Fig. S7. Concentration of UCS protein Rng3p measured by fluorescence microscopy in wt cells and temperature-sensitive *myo2-E1* cells where a point mutation inactivates most of the myosin-II even at permissive temperatures (*S17*). Wild type and mutant cells were grown in YE5S at 25°C. (A) Local accumulation of Rng3p-YFP and YFP-Myo2p at the cell-division site. Box plots show the mean (x), median (line), and outliers (o). The box represents the middle 50% data and the bars the top and bottom 25% data, respectively. Black symbols use the scale on the left. Green symbols use the scale on the right. (**B**) Global mean cytoplasmic concentrations (± 1 standard deviation) of the UCS protein Rng3p and myosin-II Myo2p.

Supplementary Tables

Table S1. *S. pombe* strains used in this study.

Strain	Genotype	Source/Reference
JW81	*h⁻ ade6-M210 leu1-32 ura4-D18*	(*S2*)
JW708	*h⁻ myp2-YFP-kanMX6 ade6-M210 leu1-32 ura4-D18*	See text
JW729	*h⁺ ade6-M210 leu1-32 ura4-D18*	(*S2*)
JW764	*h⁺ sad1-CFP-kanMX6 ade6-M210 leu1-32 ura4-D18*	(*S2*)
JW784	*myp2-YFP-kanMX6 sad1-CFP-kanMX6 ade6-M210 leu1-32 ura4-D18*	(*S2*)
JW826	*h⁺ cdc7-YFP-kanMX6 ade6-M210 leu1-32 ura4-D18*	See text
JW827	*h⁺ kanMX6-Pmyo2-YFP-myo2 ade6-M210 leu1-32 ura4-D18*	(*S2*)
JW909	*h⁺ kanMX6-Prng2-mYFP-4gly-rng2 ade6-M210 leu1-32 ura4-D18*	(*S2*)
JW910	*h⁺ kanMX6-Pcdc4-mYFP-4gly-cdc4 ade6-M210 leu1-32 ura4-D18*	(*S2*)
JW932	*h⁻ acp2-YFP-kanMX6 sad1-CFP-kanMX6 ade6-M210 leu1-32 ura4-D18*	(*S2*)
JW946	*kanMX6-Pcdc4-mYFP-4gly-cdc4 sad1-CFP-kanMX6 ade6-M210 leu1-32 ura4-D18*	(*S2*)
JW949	*h⁻ rlc1-mYFP-kanMX6 ade6-M210 leu1-32 ura4-D18*	See text
JW977	*h⁺ cdc15-mYFP-kanMX6 ade6-M210 leu1-32 ura4-D18*	See text
JW991	*rlc1-mYFP-kanMX6 sad1-CFP-kanMX6 ade6-M210 leu1-32 ura4-D18*	(*S2*)
JW1039	*h⁻ kanMX6-Pcdc15-mYFP-4gly-cdc15 ade6-M210 leu1-32 ura4-D18*	See text
JW1041	*h⁺ fim1-mYFP-kanMX6 ade6-M210 leu1-32 ura4-D18*	See text
JW1053	*h⁺ kanMX6-Pcdc15-mYFP-4gly-cdc15 sad1-CFP-kanMX6 ade6-M210 leu1-32 ura4-D18*	JW1039 x JW764
JW1063	*h⁺ kan^{s} mYFP-4gly-cdc15 ade6-M216 leu1-32 ura4-D18*	See text
JW1071	*h⁺ rgf1-mYFP-kanMX6 ade6-M210 leu1-32 ura4-D18*	See text
JW1073	*h⁺ rgf3-mYFP-kanMX6 ade6-M210 leu1-32 ura4-D18*	See text
JW1089	*h⁻ mid1-mYFP-kanMX6 ade6-M210 leu1-32 ura4-D18*	See text

JW1092	*h⁻ spn1-mYFP-kanMX6 ade6-M210 leu1-32 ura4-D18*	See text
JW1110	*h⁺ kanMX6-Pmyo2-mYFP-myo2 ade6-M210 leu1-32 ura4-D18*	See text
JW1107	*h⁺ plo1-mYFP-kanMX6 ade6-M210 leu1-32 ura4-D18*	See text
JW1141	*h⁻ sad1-mYFP-kanMX6 ade6-M210 leu1-32 ura4-D18*	See text
JW1145	*h⁻ ain1-mYFP-kanMX6 ade6-M210 leu1-32 ura4-D18*	See text
JW1168	*h⁺ chs2-mYFP-kanMX6 ade6-M210 leu1-32 ura4-D18*	See text
JW1169	*h⁺ mid2-mYFP-kanMX6 ade6-M210 leu1-32 ura4-D18*	See text
JW1170	*h⁺ pck2-mYFP-kanMX6 ade6-M210 leu1-32 ura4-D18*	See text
JW1171	*h⁺ spn4-mYFP-kanMX6 ade6-M210 leu1-32 ura4-D18*	See text
JW1206	*h⁺ ade6-M210 leu1-32 ura4-D18* + p573-81nmt1-YFP-actin	(*S18*)
JW1213	*h⁺ mid2-mEGFP-kanMX6 ade6-M210 leu1-32 ura4-D18*	See text
JW1236	*kan^s mYFP-myo2 ade6-M210 leu1-32 ura4-D18*	See text
JW1246	*kan^s mYFP-4gly-rng2 ade6-M210 leu1-32 ura4-D18*	See text
CB71	*h⁻ arc5-mYFP-kanMX6 ade6-M216 leu1-32 ura4-D18 his3-D1*	(*S19*)
CB106	*h⁺ arp2-mYFP-kanMX6 ade6-M210 leu1-32 ura4-D18 his3-D1*	(*S19*)
CB107	*h⁺ arp3-mYFP-kanMX6 ade6-M210 leu1-32 ura4-D18 his3-D1*	(*S19*)
CB108	*h⁺ arc1-mYFP-kanMX6 ade6-M210 leu1-32 ura4-D18 his3-D1*	(*S19*)
CB109	*h⁺ arc3-mYFP-kanMX6 ade6-M210 leu1-32 ura4-D18 his3-D1*	(*S19*)
KV60	*h⁺ acp2-YFP-kanMX6 ade6-M210 leu1-32 ura4-D18*	(*S2, S18*)
KV346	*h⁻ cdc12-3YFP-kanMX6 ade6-M216 leu1-32 ura4-D18 his3-D1*	(*S20*)
MLP660	*h⁻ rng3-3YFP-kanMX6 leu1-32*	(*S17*)
MLP683	*h⁻ rng3-3YFP- kanMX6 myo2-E1 leu1-32*	(*S21*)

Table S2. Comparison of protein abundance between *S. pombe* and *S. cerevisiae*.

Protein in *S. pombe*	Mean molecules per cell in *S. pombe*	Molecules per cell *S. pombe* /*S. cerevisiae*	Mean molecules per cell in *S. cerevisiae* (*S22*)	Homologue in *S. cerevisiae*
Actin patch proteins				
Actin Act1p	1.43×10^6	6.4*	NA†	Act1p
Arp2 (Arp2p)	46,600	7.0	6,650	Arp2p
Arp3 (Arp3p)	66,700	10.0	6,650	Arp3p
ARPC1 (Arc1p/Sop2p)	40,300		NA	Arc40p
ARPC3 (Arc3p/Arc21p)	38,700	20.2	1,920	Arc18p
ARPC5 (Arc5p/Arc16p)	30,500	10.0	3,060	Arc15p
Capping protein Acp2p	19,200	2.8	6,770	Cap2p
Fimbrin Fim1p	86,500	24.6	3,510	Sac6p
Spindle pole body proteins				
SPB protein Sad1p	3,300		NA	Mps3p
Polo kinase Plo1p	6,600	4.5	1,480	Cdc5p
SIN kinase Cdc7p	4,000	16.8	238	Cdc15p
Cytokinesis proteins				
Anillin-like Mid1p	2,100			NH‡
Myosin-II Myo2p	7,300	3.4	2,140	Myo1p
Myosin-II ELC Cdc4p	77,000		NA	Mlc1p
Myosin-II RLC Rlc1p	9,600	8.5	1,130	Mlc2p
IQGAP Rng2p	2,700	9.7	279	Iqg1p/Cyk1p
PCH protein Cdc15p	35,600	182.6	195	Hof1p/Cyk2p

Formin Cdc12p	600	3.6; 2.3	166; 259	Bni1p; Bnr1p
UCS protein Rng3p	1,900	0.6	3,410	She4p/Dim1p
Alpha-actinin Ain1p	3,600			NH
Myosin-II Myp2p	6,100			NH
Septin Spn1p	10,300		NA	Cdc3p
Septin Spn4p	8,100	6.9	1,170	Cdc12p
Anillin-like Mid2p	1,800	1.1	1,600	Bud4p
Protein kinase C Pck2p	4,300	1.5	2,950	Ypk1p
Rho GEF Rgf1p	4,300	16.6	259	Rom2p
Rho GEF Rgf3p	3,200		NA	Tus1p
Chitin synthase Chs2p	2,100		NA	Chs2p

*The ratio was calculated using the global actin concentration of 5.3 μM (without excluding volume) (*S23*) and cell volume of 70 μm^3 (*S24*) of haploid *S. cerevisiae*.

†No data available (*S22*).

‡No obvious homologue in *S. cerevisiae*.

Supplementary References and Notes

S1. J. Bähler *et al.*, *Yeast* **14**, 943 (1998).
S2. J.-Q. Wu, J. R. Kuhn, D. R. Kovar, T. D. Pollard, *Dev. Cell* **5**, 723 (2003).
S3. K. Hirschberg *et al.*, *J. Cell Biol.* **143**, 1485 (1998).
S4. D. A. Zacharias, J. D. Violin, A. C. Newton, R. Y. Tsien, *Science* **296**, 913 (2002).
S5. D. B. Hoffman, C. G. Pearson, T. J. Yen, B. J. Howell, E. D. Salmon, *Mol. Biol. Cell* **12**, 1995 (2001).
S6. D. W. Piston, G. H. Patterson, S. M. Knobel, *Methods Cell Biol.* **58**, 31 (1999).
S7. A. Downs, T. D. Pollard, unpublished data.
S8. M. Morphew, J. R. McIntosh, unpublished data.
S9. T. Kanbe, I. Kobayashi, K. Tanaka, *J. Cell Sci.* **94**, 647 (1989).
S10. R. Ding, R. R. West, D. M. Morphew, B. R. Oakley, J. R. McIntosh, *Mol. Biol. Cell* **8**, 1461 (1997).
S11. S. Uzawa *et al.*, *Mol. Biol. Cell* **15**, 5219 (2004).
S12. T. Takagi, S. A. Ishijima, H. Ochi, M. Osumi, *J. Electron Microsc.* **52**, 161 (2003).
S13. R. D. Mullins, W. F. Stafford, T. D. Pollard, *J. Cell Biol.* **136**, 331 (1997).
S14. R.D. Mullins, J. Kelleher, T. D. Pollard, unpublished data.
S15. N. I. Naqvi, K. C. Y. Wong, X. Tang, M. K. Balasubramanian, *Nat. Cell Biol.* **2**, 855 (2000).
S16. X. Le Goff, F. Motegi, E. Salimova, I. Mabuchi, V. Simanis, *J. Cell Sci.* **113**, 4157 (2000).
S17. M. Lord, T. D. Pollard, *J. Cell Biol.* **167**, 315 (2004).
S18. D. R. Kovar, J.-Q. Wu, T. D. Pollard, *Mol. Biol. Cell* **16**, 2313 (2005).
S19. C. C. Beltzner, T. D. Pollard, unpublished data.
S20. D. R. Kovar, T. D. Pollard, unpublished data.
S21. M. Lord, T. D. Pollard, unpublished data.
S22. S. Ghaemmaghami *et al.*, *Nature* **425**, 737 (2003).
S23. K. Kim, A. Yamashita, M. A. Wear, Y. Maeda, J. A. Cooper, *J. Cell Biol.* **164**, 567 (2004).
S24. F. Sherman, *Methods Enzymol.* **350**, 3 (2002).